XLIII CILAMCE
21–25, November, 2022
FOZ DO IGUAÇU – PR – BRAZIL

A refined plastic-hinge-based formulation for advanced analysis of CFST columns: a co-rotational proposition

Ígor J.M. Lemes[1], Pedro H.A. Lima[2], Ricardo A.M. Silveira[2], Rafael C. Barros[3], Jéssica L. Silva[4]

[1]*Dept. of Engineering, Federal University of Lavras*
Campus Universitário, 37200-900, Lavras, MG, Brazil
igor.lemes@ufla.br
[2]*Dept. of Civil Engineering, Federal University of Ouro Preto*
Campus Universitário s/n, Morro do Cruzeiro, 35400-000, Ouro Preto, MG, Brazil
pedro.hal@aluno.ufop.edu.br, ricardo@ufop.edu.br
[3]*Sereng Engineering & Consulting*
34006-056, Nova Lima, Minas Gerais, Brazil
rafaelcesario@hotmail.com
[4]*Brazilian Air Force, Ministry of Defense*
36205-058, Barbacena, Minas Gerais, Brazil
jessicalorrany05@hotmail.com

Abstract. The present work aims to propose a lumped plasticity-based numerical formulation for the non-linear analysis of concrete-filled steel tubular (CFST) columns. The study is divided into two main parts: cross-sectional analysis and global structural analysis. The local analysis is made by means of the strain compatibility method. Thus, the moment-curvature relationship is evaluated by an incremental-iterative process. Through of this methodology, the limits of uncracked, cracked, elastic, inelastic and bearing capacity are determined for various axial efforts. Thus, the NM diagram is calculated with three curves and five regimes to describe the cross-section flexural stiffness. For the precise evaluation of this numerical procedure, the materials constitutive relationships are explicitly considered. For the global analysis, the co-rotational-based approach is used to describe the finite element formulation allowing large displacements and rotations in the numerical model. This approach is coupled to rotational pseudo-springs at the ends of the finite element, where the gradual loss of stiffness was determined by combining the normal force and bending moment (NM) in the cross-section. The numerical results were compared with experimental results [15]. In average, the results found present an error of 0.1% in relation to the data obtained in the laboratory, demonstrating the accuracy of the proposed numerical formulation.

Keywords: CFST, lumped plasticity, NM diagram, non-linear analysis, pseudo-springs.

1 Introduction

Among the most used materials in civil construction, concrete and steel stand out. The association of these materials aims, fundamentally, for the best physical and mechanical use of them. Steel-concrete composite columns have high load–carrying capacity and stiffness if compared to the usual reinforced concrete and bare steel elements. Moon et al. [1] highlighted that the external steel tube of the concrete-filled composite columns (CFST) is also used to replace the formwork during the construction phase, speeding up construction time and promoting cost-savings.

Over the years, several works developed experimental studies aiming accurately evaluating the load capacity and behavior of the CFST [2, 3] composite columns. These researches demonstrated that several factors directly influence the structure's load–carrying capacity and its behavior in general. Experimental research, in general, requires a high cost. In this scenario, numerical analysis models are highlighted.

Refined plastic-hinge method (RPHM) is a simpler methodology to make advanced analysis of steel, reinforced concrete and steel concrete composite structures. The classical RPHM approach starts from a hybrid finite element with pseudo-springs at the ends of the finite elements, such that the stiffness degradation of these springs is responsible for introducing the material's non-linearity under three regimes: linear-elastic, elastoplastic and plastic [4]. The linear-elastic regime contradicts the non-linear behavior of concrete under compression, and there is no consideration of cracking in this methodology. Thus, concrete cracking is introduced in approximate positions

in the model through an empirical coefficient to reduce the stiffness of the concrete element [5–7]. To correct the problems generated by the concrete cracking within the RPHM, Lemes et al. [8] proposed the explicit consideration of cracking through the imposition of cracked and uncracked regimes within the interaction curves. Thus, when the cracking starts, the moment of inertia of the cross-section is reduced as per Branson and Metz's [9] equation.

The present study aims to develop a plastic-fiber-hinge-based numerical formulation for the non-linear simulation of CFST columns. For this, an important contribution of this study is to promote the coupling of the co-rotational finite element using RPHM. To include concrete cracking here, second moment of area of the section will be addressed via the Branson and Metz proposition [9]. On the other hand, the plastification effects will be inserted through rotational pseudo-springs, which will introduce in the numerical model the loss of stiffness due to the plastic behavior of steel and concrete. The cross-sectional analysis is done via strain compatibility method [8, 10–12].

2 Co-rotational formulation

2.1 Element formulation

If the structural element presents large displacements and/or large rotations, the global degrees of freedom contain the rigid motion and the deformational part; the co-rotational approach aims to separate these parts. This approach is convenient for establishing the relationship between the local and global variables. The relation between global and local degrees of freedom is obtained by a simple differentiation of the co-rotational displacements described in the function of global displacements.

Starting from the virtual work principle and correlating global and local variables using the transformation matrix $\mathbf{B}$ [10], the differentiation of global forces vector, $\mathbf{f}_g$, in relation to the global displacements vector,$\mathbf{u}_g$, results in the global stiffness matrix, $\mathbf{K}_g$. This matrix is described as follows:

$$\mathbf{K}_g = \frac{\Delta \mathbf{f}_g}{\Delta \mathbf{u}_g} = \mathbf{B}^T \mathbf{K}_l \mathbf{B} + \frac{\mathbf{z}\mathbf{z}^T}{L} N + \frac{1}{L^2} \left(\mathbf{r}\mathbf{z}^T + \mathbf{z}\mathbf{r}^T \right) (M_i + M_j) \tag{1}$$

where $\mathbf{K}_l$, N, M_i and M_j are the stiffness matrix and the internal forces in the local system, respectively, L is the finite element length, z and r are geometrical vectors. For more detail in how to obtain this matrix, see [11].

2.2 Stiffness Matrix in Local System ($\mathbf{K}_l$)

Lower-order interpolation functions are associated with locking phenomena in displacement-based FE formulations. Tang et al. [13] pointed out that membrane locking would arise when a straight beam-column element with low-order axial displacement interpolation is used in the geometrical non-linear analysis.

Using the degenerated form of the Green strain and the curvature based on the Euler-Bernoulli theory, considering locking-free displacement interpolations functions [11], and assuming here the material elastic behavior and that applied load is conservative and nodal, the system potential energy may be expressed by the strain energy U and external work done W, that is,

$$\Pi = U - W = \frac{1}{2} EA \int_0^L \varepsilon^2 dx + \frac{1}{2} EI \int_0^L \Phi^2 dx - \sum_{i=1}^{3} f_{l,i} u_{l,i} \tag{2}$$

where E is the modulus of elasticity and A and I are area and moment of inertia, respectively, ε is the axial strain, Φ is the curvature and $f_{l,i}$ and $u_{l,i}$ are the nodal forces and displacements in local system. By the principle of stationary potential energy, the first variation on the function yields the equilibrium equations, that is [13]:

$$\Delta \Pi = \left(\frac{\partial U}{\partial \mathbf{u}_l} - \mathbf{f}_l \right) \Delta \mathbf{u}_l = 0 \tag{3}$$

being the first variation of strain energy, U, resulting in the local internal forces vector, $\mathbf{f}_l$, as follows:

$$\mathbf{f}_l = \frac{\partial U}{\partial \mathbf{u}_l} \tag{4}$$

and the local tangent stiffness matrix, $\mathbf{K}_l$, is obtained as the second variation of strain energy, variation of $\mathbf{f}_l$ as follows:

$$\mathbf{K}_l = \frac{\partial^2 U}{\partial \mathbf{u}_l^2} = \frac{\partial \mathbf{f}_l}{\partial \mathbf{u}_l} \tag{5}$$

3 Lumped plasticity approach

In the present work, the displacement-based formulation with concentrated plasticity in the nodal points is applied. In this case, the axial and flexural stiffness degradation occurs exclusively at the FE nodes. Then, the method is presented, introducing the material non-linearity only. Some considerations and simplifications of this formulation can be seen in [8].

In the structural system modelling, the hybrid beam-column finite element of length L, delimited by nodal points i and j (Figure 1), is used. This element has zero-length pseudo rotational springs at its ends, which are responsible for the plasticity simulation by means of the parameter S_p, discussed in Section 4. The finite element is referenced to the co-rotational system where the degrees of freedom are the rotations at nodes i and j, given by θ_i and θ_j, and the axial displacement in j, δ. The terms M_i, M_j and N represent the bending moments and the axial force in the respective degrees of freedom.

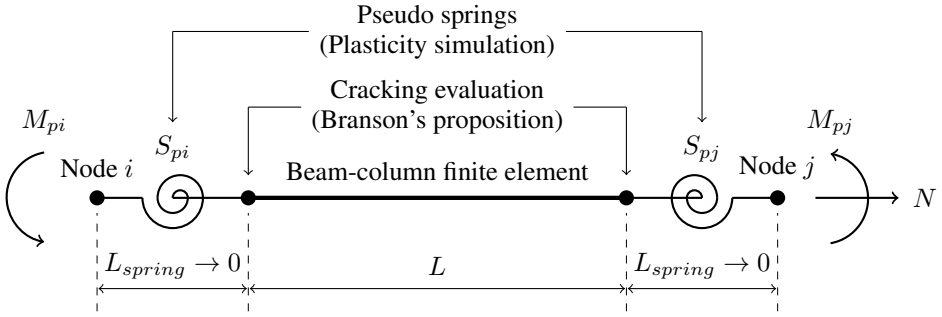

Figure 1. Finite element with pseudo-springs

$$\begin{Bmatrix} \Delta N \\ \Delta M_{pi} \\ \Delta M_{pj} \end{Bmatrix} = \begin{bmatrix} k_{11} & 0 & 0 \\ 0 & S_{pi} - \dfrac{S_{pi}^2\,(S_{pj}+k_{33})}{\beta} & \dfrac{S_{pi}k_{23}S_{pj}}{\beta} \\ 0 & \dfrac{S_{pj}k_{32}S_{pi}}{\beta} & S_{pj} - \dfrac{S_{pj}^2\,(S_{pi}+k_{22})}{\beta} \end{bmatrix} \begin{Bmatrix} \Delta\delta \\ \Delta\theta_{pi} \\ \Delta\theta_{pj} \end{Bmatrix} \tag{6}$$

in which $\beta = (S_{pi} + k_{22})\,(S_{pj} + k_{33}) - k_{32}k_{23}$.

The terms k_{11}, k_{22}, k_{23}, k_{32}, and k_{33} are components of the beam-column stiffness matrix element, without the pseudo-springs, described as [8]:

$$\begin{aligned} k_{11} &= \frac{E_s A}{L} & k_{22} &= \frac{E_s\,(3I_{eff,i} + I_{eff,j})}{L} \\ k_{23} = k_{32} &= \frac{E_s\,(I_{eff,i} + I_{eff,j})}{L} & k_{33} &= \frac{E_s\,(I_{eff,i} + 3I_{eff,j})}{L} \end{aligned} \tag{7}$$

where E_s is the steel modulus of elasticity, A is the homogenized area of the section, I_{eff} is the modulus of inertia as discussed on Section 5, measured in nodes i and j, and L is the finite element length.

4 Pseudo-spring flexural stiffness

The limits of uncracked, elastic or plastic states are defined by the moment-curvature relationship [12]. In this non-linear procedure, the initial cracking moment M_{cr}, the initial yield moment M_{er} and the full yield moment M_{pr} can be easily obtained.

Figure 2 illustrates three interaction curves for a specific cross-section: the full yield curve – indicates the bearing capacity; the initial yield curve – defines the elastic region; and the initial cracking curve – delimits the uncracked state of the cross-section. These curves are the result of a combination of axial force and a bending moment acting around one of the main axes bending. For bare steel or steel-concrete composite columns, the procedure to obtain these three curves is described in Lemes et al. [8].

In Figure 2, it is also possible to observe four regions. Thus, expression definitions for the simulation of pseudo-spring stiffness in each of the described regions are required.

According to the classical RPHM, three equations define the pseudo-spring stiffness for the previously mentioned regions. In regions 1 and 2, it is observed that the section is in an elastic regime. In regions 3 and 4, there

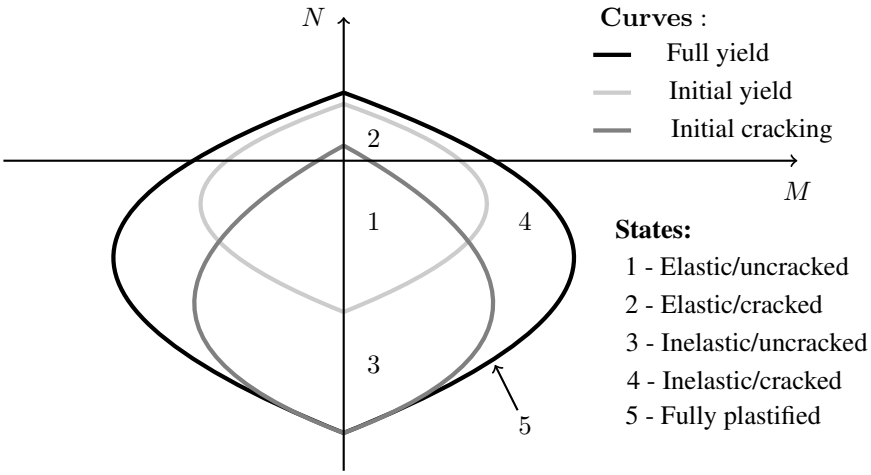

Figure 2. Interaction curves for cross section flexural stiffness degradation

can be noticed that the section is in a stiffness degradation process due to plastic strains. And finally, for when the fully plastified section occurs (region 5). For a given axial force-bending moment combination, S_p is defined as follow:

$$\begin{aligned} &\text{if} \quad M \leq M_{er}: \quad S_p = 1 \times 10^{10} \\ &\text{if} \quad M_{er} \leq M \leq M_{pr}: \quad S_p = \frac{E_s I_{eff}}{L}\left(\frac{M_{pr} - M}{M - M_{er}}\right) \\ &\text{if} \quad M_{pr} \leq M: \quad S_p = 1 \times 10^{-10} \end{aligned} \tag{8}$$

in which L is the finite element length and $E_s I_{eff}$ is the section's flexural stiffness, considering the cracking, as discussed below.

Note that, by the value described in Eq. 8, there is no possibility of simulating cracking in the elastic regime. This adjustment is made in the following section.

5 Cracking effect in the concrete section

Branson and Metz [9] proposed a simple equation for the effective moment of inertia evaluation of RC sections in a cracking state. According to these authors, the effective moment of inertia,$I_{eff,c}$, is given by:

$$\begin{aligned} &\text{if} \quad M \leq M_{cr}: \quad I_{eff,c} = I_c \\ &\text{if} \quad M > M_{cr}: \quad I_{eff,c} = \left(\frac{M_{cr}}{M}\right)^3 I_c + \left[1 - \left(\frac{M_{cr}}{M}\right)^3\right] I_{cr} \quad I_{eff} \leq I_c \end{aligned} \tag{9}$$

where M_{cr} and M are, respectively, the initial cracking bending moment and the bending moment acting on the section, I_c is the moment of inertia of the gross section, and I_{cr} is the cracked moment of inertia of the section evaluated in the critical point of moment-curvature relationship [8].

In order to enable the application of a single moment of inertia for the three components of the cross-section within the stiffness matrix, homogenization was carried out:

$$I_{eff} = I_s + \frac{E_r}{E_s} I_r + \frac{E_c}{E_s} I_{eff,c} \tag{10}$$

where E_r and I_r are the modulus of elasticity and the second moment of area of the reinforcement bars that may be present in the concrete component; E_s and I_s are the same properties of the steel section, respectively; and $I_{eff,c}$ is the effective moment of inertia of the concrete considering the cracking effects.

It is noteworthy that the concrete's modulus of elasticity, E_c, is obtained in a particular manner. When the initial tangential elastic modulus (E_{ci}), illustrated in Figure 3, is used as E_c, its value is overestimated. This is because due to the non-linear behavior of concrete under compression, low strain rates imply a reduction in the

modulus of elasticity. On the other hand, the use of the elastic secant modulus E_{csi}, between 0 and $(\varepsilon_{cin}, f_{cin})$ [14], generates conservative results for low strain values. Accordingly, for the global structural analysis, E_c was defined as the mean value between E_{ci} and E_{csi}. The values of ε_{cin} and f_{cin} can be easily calculated considering Hooke's equation ($f_c = \varepsilon E_c$) and constitutive relationship [6], resulting in $\varepsilon_{cin} = \varepsilon_{ci}/2$ and $f_{cin} = 0.75 f_c$. Thus, $E_c = 1.5 f_c/\varepsilon_{ci}$.

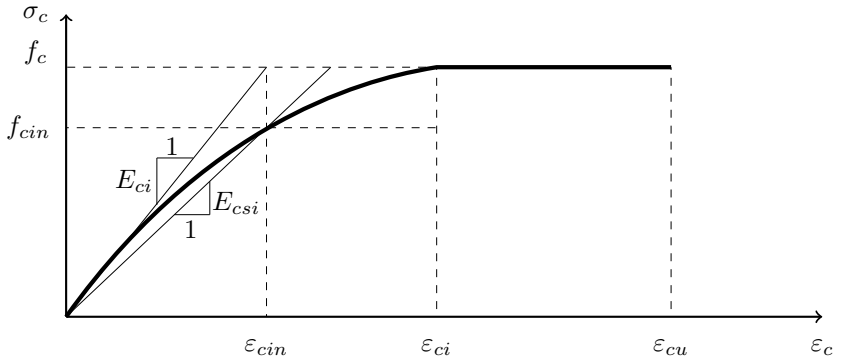

Figure 3. Concrete stress-strain relationship under compression: elastic limit strain and modulus of elasticity

Finally, after inserting the effects of yielding (through the refined plastic-hinge method) and cracking in the stiffness matrix, it is possible to determine the force–displacement curve seeking the most convergent results for the actual behavior of the structure.

6 Numerical applications

Seven tested steel–concrete composite columns [15] were simulated in this subsection. Some authors [5, 16] used these experimental results to test their RPHM-based formulations. The simulated model consists of a simply supported column without an initial geometric imperfection. A load eccentricity was introduced to the system considering bending moments at both top and base of the column, as shown in Figure 4. Four finite elements were used. The geometric and materials properties of each specimen are presented in Table 1.

Table 1. Coefficients in constitutive relations

Specimen	L	e	d	t	f_{ys}	E_s	f_c	P_{test}	P_p	$\frac{P_p}{P_{test}}$
	cm	cm	cm	cm	kN/cm^2	kN/cm^2	kN/cm^2	kN	kN	
M1	332.74	4.76	16.94	0.511	30.9	20700	5.553	621.8	632.911	1.018
M2	332.74	3.81	16.92	0.526	30.9	20700	5.400	701.5	723.997	1.032
M3	332.74	4.76	16.89	0.566	29.5	20700	4.247	599.8	581.973	0.970
M4	332.74	4.76	16.84	0.655	29.8	20700	3.800	624.7	611.523	0.979
M5	**332.74**	**4.76**	**16.94**	**0.719**	**31.2**	**20700**	**3.200**	**652.6**	**645.708**	**0.989**
M6	332.74	3.81	16.94	0.729	31.2	20700	3.318	738.3	742.206	1.005
M7	330.20	4.76	16.89	0.881	32.3	20700	3.306	757.3	754.487	0.996

All columns were numerically simulated and in Figure 4, only the equilibrium path of the specimen M5 is illustrated, since it is the only curve provided by Neogi et al. [15]. This figure shows the proximity between numerical and experimental results. It also verifies the agreement in the structure stiffness drop from the beginning of the cracking process, which occurs when the load is equal to 231.849 kN. For this formulation, the section yield process beginning when the load is equal to 458.78 kN. Another point to be highlighted is the precision of the formulation in the evaluation of the structure's post-critical behavior, which is compatible with what was experimentally obtained. Table 1 also presents the critical loads obtained here, P_p, and they are compared with the experimental results, P_{test}. The table also compares the values of the loads obtained here with those found in the literature. The low average difference, P_{test} (0.1%), points to the reliability of numerical analyses presented for CFST columns under axial force and bending moment.

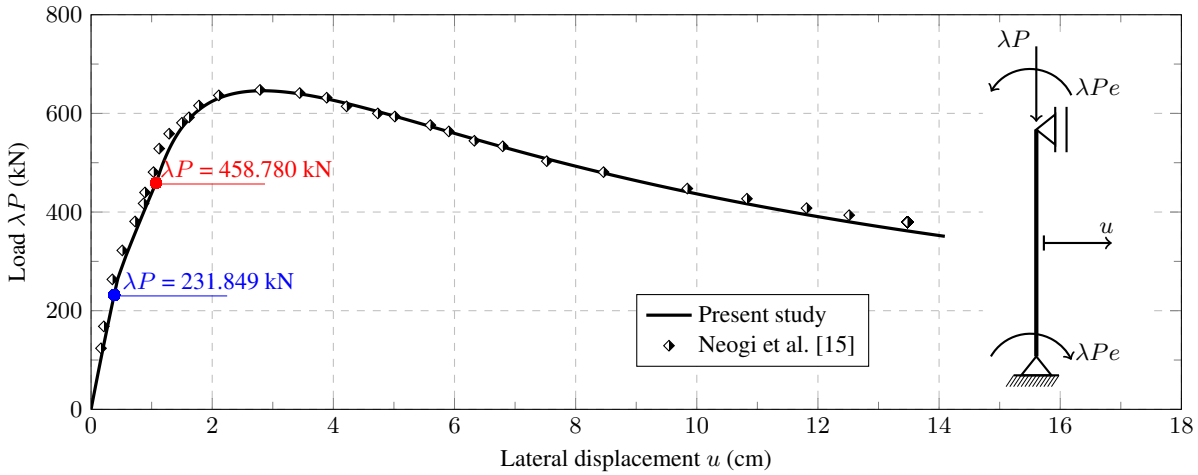

Figure 4. Concrete-filled circular hollow steel columns: equilibrium path of M5

7 Conclusions

The use of the refined plastic hinge method for steel-concrete composite structures is not new. The present study proposed to include a precise approach to geometric non-linearity via co-rotational proposition. Furthermore, the inclusion of cracking effects by Branson's equation and the definition of a uncracked section is important for the correct evaluation of the cross-sectional stiffness. The strain compatibility method produces a precise cross-sectional analysis, where several conditions are analyzed: uncracked, cracked, elastic, inelastic and ultimate strength. The interaction curves, built by a numerical method that explicitly considers the constitutive relationships, are closer to reality since simplified equations are not used.

This article focused on the results of the analysis of seven CFST columns. The numerical results were compared with experimental results [15]. In average, the results found present an error of 0.1% in relation to the data obtained in the laboratory, demonstrating the accuracy of the formulation. Furthermore, it is possible to observe a low standard deviation, showing the consistency of the formulation precision in all seven analyses.

With the consolidation of the data presented here, the aim is to expand the formulation to enable the analysis of steel-concrete composite frames with semi-rigid connections, in addition to including the effect of partial interaction in this approach (considering the inclusion of conditions for the analysis of composite beams). Furthermore, objective is also to expand the formulation to the three-dimensional context, and to analyze the specificities of different cross-sections.

Acknowledgements. The authors would like to thank CAPES and CNPq (Federal Research Agencies), Fapemig (Minas Gerais State Research Agency), UFLA and UFOP for their support during the development of this work.

Authorship statement. The authors hereby confirm that they are the sole liable persons responsible for the authorship of this work, and that all material that has been herein included as part of the present paper is either the property (and authorship) of the authors, or has the permission of the owners to be included here.

References

[1] J. Moon, C. W. Roeder, D. E. Lehman, and H.-E. Lee. Analytical modeling of bending of circular concrete-filled steel tubes. *Engineering Structures*, vol. 42, pp. 349–361, 2012.

[2] Y.-F. Yang and L.-H. Han. Behaviour of concrete filled steel tubular (cfst) stub columns under eccentric partial compression. *Thin-Walled Structures*, vol. 49, pp. 379–395, 2011.

[3] X. Qu, Z. Chen, and G. Sun. Experimental study of rectangular cfst columns subjected to eccentric loading. *Thin-Walled Structures*, vol. 64, pp. 83–93, 2013.

[4] S. L. Chan and P. Chui. *Non-linear static an cyclic analysis of steel frames with semi-rigid connections*. Elsevier, Oxford, 2000.

[5] M. Fong and S. L. Chan. Advanced analysis of steel-concrete composite beam-columns by refined plastic-hinge method. *International Journal of Structural Stability and Dynamics*, vol. 12, n. 6, 2012.

[6] Í. J. M. Lemes, A. R. D. Silva, R. A. M. Silveira, and P. A. S. Rocha. Determinação da capacidade resistente de elementos estruturais mistos através do método da rótula plástica refinado. *Revista Internacional de Métodos Numéricos para Cálculo y Diseño en Ingeniería*, vol. 33, n. 1-2, pp. 24–34, 2017a.
[7] Í. J. M. Lemes, A. R. D. Silva, R. A. M. Silveira, and P. A. S. Rocha. Numerical analysis of nonlinear behavior of steel concreto composite structures. *Ibracon Structures and Materials Journal*, vol. 10, n. 1, pp. 53–83, 2017b.
[8] Í. J. M. Lemes, R. C. Barros, R. A. M. Silveira, A. R. D. Silva, and P. A. S. Rocha. Numerical analysis of rc plane structures: a concentrated nonlinear effect approach. *Latin American Journal of Solids and Structures*, vol. 15, n. 2, 2018.
[9] D. Branson and G. Metz. Instantaneous and time-dependent deflections of simple and continuous reinforced concrete beams. Technical report, Auburn: Dept. of Civil Engineering Auburn Research Foundation, Auburn University, Auburn: Dept. of Civil Engineering and Auburn Research Foundation, Auburn University, 1963.
[10] Í. J. M. Lemes, L. E. S. Dias, R. A. M. Silveira, A. R. Silva, and T. A. Carvalho. Numerical analysis of steel–concrete composite beams with partial interaction: A plastic-hinge approach. *Engineering Structures*, vol. 248, pp. 113256, 2021.
[11] J. L. Silva, L. R. R. M. Deus, Í. J. M. Lemes, , and R. A. M. Silveira. Plastic analysis of steel arches and framed structures with various cross sections. *Steel and Composite Structures*, vol. 38, n. 3, pp. 257–270, 2021.
[12] Í. J. M. Lemes, R. A. M. Silveira, A. R. D. Silva, and P. A. S. Rocha. Nonlinear analysis of two-dimensional steel, reinforced concrete and composite steel-concrete structures via coupling SCM/RPHM. *Engineering Structures*, vol. 147, pp. 12–26, 2017.
[13] Y. Q. Tang, Z. H. Zhou, and S. L. Chan. Nonlinear beam-column element under consistent deformation. *International Journal of Structural Stability and Dynamics*, vol. 15, n. 5, pp. 1450068, 2015.
[14] B. Izzuddin and D. L. Smith. Efficient nonlinear analysis of elasto-plastic 3d r/c frames using adaptive techniques. *Computers & Structures*, vol. 78, n. 4, pp. 549–573, 2000.
[15] P. Neogi, H. Sen, and J. Chapman. Concrete-filled tubular steel columns under eccentric loading. *The Structural Engineer*, vol. 47, n. 5, pp. 187–195, 1969.
[16] S. W. Liu, Y. P. Liu, and S. L. Chan. Advanced analysis of hybrid steel and concrete frames part 2: Refined plastic hinge and advanced analysis. *Journal of Constructional Steel Research*, vol. 70, pp. 337–349, 2012b.